Cascaded Digital Beamforming on Receive with the ROSE-L Multichannel SAR System for Along-Track Deformation Retrieval

Simon Trumpf, Pau Prats-Iraola, Alberto Moreira November 2025

This is the author's version, page numbering might differ from the publisher's version. Please visit https://doi.org/10.1109/lgrs.2025.3638247 for the publisher's version. Copyright is with IEEE.

Cascaded Digital Beamforming on Receive with the ROSE-L Multichannel SAR System for Along-Track Deformation Retrieval

Simon Trumpf, Pau Prats-Iraola, Fellow, IEEE, Alberto Moreira, Fellow, IEEE

Abstract—The upcoming ROSE-L synthetic aperture radar (SAR) mission employs a large array antenna with multiple azimuth channels on receive, enabling the usage of different beamforming algorithms on ground. Recent analyses have shown the feasibility of retrieving along-track deformation with the ROSE-L system using two-look ScanSAR, however with limited accuracy towards the burst edges due to reduced antenna gain and increased azimuth ambiguities. With beamforming being a state-of-the-art technique to adapt the characteristics of antenna arrays, this letter presents and analyses a cascaded beamforming approach to improve the retrieval performance. It therefore analyses azimuth ambiguities and system noise and their impact on the performance. It is shown that the increased SNR leads to an increased interferometric coherence for scenes with low SNR, thus improving the accuracy of the retrieved along-track deformation in this case.

Index Terms—Synthetic aperture radar (SAR) interferometry, two-look ScanSAR, digital beamforming

I. INTRODUCTION

THE estimation of three-dimensional ground deformations using interferometric techniques with spaceborne Synthetic Aperture Radar (SAR) is often limited by the nearpolar orbits of most SAR satellites. As the measurements using differential SAR interferometry are only sensitive to deformations along the line of sight (LOS) and the LOS is primarily oriented in East-West and vertical directions for moderate latitudes, the sensitivity for North-South deformations in these regions is low [1]. In case advanced interferometric wide-swath SAR acquisition modes [2] like ScanSAR or TOPS are used, this limitation can be partially overcome by interferometrically exploiting the overlap of two adjacent bursts, referred to as two-look ScanSAR or two-look TOPS and as demonstrated with the TerraSAR-X [3], Sentinel-1 [4], [5] and ALOS systems [6]. The two-look ScanSAR approach is also applicable with the upcoming Radar Observing System for Europe in L-Band (ROSE-L) [7], where, due to the large available azimuth Doppler bandwidth, the two looks can be obtained without deteriorating the azimuth resolution. A performance analysis of such processing approach has been presented in [8] and system adjustments for improved along-track deformation estimation have been proposed in [9]. ROSE-L is a mission in the frame of the Copernicus Sentinel Expansion Missions led by the European Commission and supported by the European Space Agency. Besides ScanSAR,

The authors are with the Microwave and Radar Institute, German Aerospace Center (DLR), 82234 Wessling, Germany (email: Simon.Trumpf@dlr.de).

ROSE-L uses multiple azimuth phase centers with an antenna consisting of five subapertures in azimuth. As the signals of the channels in azimuth are transmitted to ground, different strategies can be applied for the recombination in processing. The common approach to reconstruct a single signal from multiple channels in azimuth has been presented in [10] and is widely used in SAR systems. Alternative reconstruction approaches could be applied to reduce the system noise, as the system provides an azimuth bandwidth exceeding the requirement for the two-look ScanSAR processing. Cascaded beamforming approaches, combining the reconstruction with a maximum beam steering for increasing the SNR, could prove to be advantageous concerning the retrieval accuracy when compared to the azimuth reconstruction with all channels [11]. This article presents and analyses such cascaded recombination approaches and compares them with the conventional reconstruction using all sub-apertures. It hereby builds on the performance analyses and metrics described in [8].

The article is structured as follows. Section II introduces the analyzed beamforming networks. Section III presents an analytic performance estimation for the azimuth deformation retrieval. Finally, conclusions are drawn in Section IV.

II. CASCADED BEAMFORMING APPROACH

The cascaded beamforming approach consists of an azimuth reconstruction step and an additional beamforming step. Note that, in contrast to most literature on beamforming, this article presents the relevant equations as functions of the local azimuth Doppler frequency $f_{\rm az}$ instead of functions of the antenna angle of arrival Θ . Both measures are equivalent in SAR and can be converted with an approximation using the satellite velocity $v_{\rm s}$ and the wavelength λ with [12]

$$f_{\rm az} = \frac{2 \cdot v_{\rm s}}{\lambda} \cdot \sin \Theta. \tag{1}$$

The azimuth reconstruction approach uses N different sets of filters, which combine the N different channel signals to remove aliasing on an interval of width $B_{\rm rec} = N \cdot {\rm PRF_{ch}}$ in the azimuth Doppler bandwidth, where ${\rm PRF_{ch}}$ is the pulse repetition frequency. The algorithm has been presented and thoroughly analyzed in [10]. It can be interpreted as N beamforming networks, which are configured to steer nulls of the combined antenna pattern to ambiguous azimuth Doppler frequencies. The reconstruction can be expressed as system of

$$\begin{bmatrix} u(f_0) \\ \vdots \\ u(f_{N-1}) \end{bmatrix} = \begin{bmatrix} P_1(f_0) & \cdots & P_N(f_0) \\ \vdots & \ddots & \vdots \\ P_1(f_{N-1}) & \cdots & P_N(f_{N-1}) \end{bmatrix} \cdot \begin{bmatrix} u_1(f_0) \\ \vdots \\ u_N(f_0) \end{bmatrix}.$$
(2)

The complex-valued filter weights $P_n(f_k)$ are weights for the nth channel signal to reconstruct the kth frequency interval with $f_k = f_0 + k \cdot \mathrm{PRF_{ch}}$, where f_0 represents the corresponding azimuth Doppler frequency in the aliased signal.

The main signal parameters limiting the along-track deformation retrieval with the two-look ScanSAR technique are the signal-to-noise ratio (SNR) and the azimuth-ambiguity-to-signal ratio (AASR). The reconstruction uses the channel diversity to suppress azimuth ambiguities while potentially increasing noise levels. For cases where noise levels are the more crucial factor, different beamforming techniques can be applied for reducing noise rather than removing ambiguities. A certain reconstructed bandwidth is still required to ensure full two-look coverage, such that the condition $B_{\rm rec} \geq B_{\rm 2look}$ is fulfilled, with $B_{\rm rec}$ representing the total reconstructed signal bandwidth and $B_{\rm 2look}$ the signal bandwidth required to obtain full two-look coverage. Hence, the reconstruction cannot be

TABLE I: Simulation parameters for ROSE-L.

Number of channels	N_{ch}	5
Carrier wavelength	λ	$24\mathrm{cm}$
Satellite velocity	$v_{ m s}$	$7142.76\mathrm{ms^{-1}}$
Sub-swath		nearest
Incident angle	$\theta_{ m inc}$	32°
Channel pulse repetition frequency	PRF_{ch}	$1567.85\mathrm{Hz}$
Slant range distance of closest approach	R_0	$804\mathrm{km}$
Bandwidth of a target	B_{target}	$635\mathrm{Hz}$
Bandwidth of a two-look burst	$B_{2\mathrm{look}}$	$4611\mathrm{Hz}$

fully replaced with the alternative beamforming approach, but a cascaded system is created. This cascaded system first applies the azimuth reconstruction using subsequent subsets of N channels, where N has to be chosen large enough so that full two-look coverage of the bursts is maintained, fulfilling $N \geq N_{\min}$, with

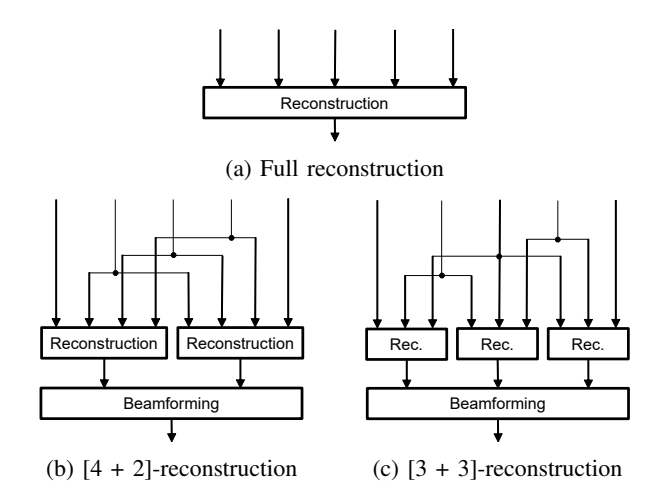
$$N_{\min} = \left\lceil \frac{B_{2\text{look}}}{\text{PRF}_{\text{ch}}} \right\rceil. \tag{3}$$

In a second stage, the SNR is increased by using beamforming with the resulting M channels, with $M=N_{\rm ch}-N+1$.

For the assumed system parameters as given in Table I, $N_{\rm min}=3$ applies. In the following, all cascaded systems which fulfill the requirement will be analyzed, which are given in Table II.

TABLE II: Test cases with full, [4 + 2] and [3 + 3] reconstruction.

Label	N	M
Full reconstruction	5	1
[4 + 2]-reconstruction	4	2
[3 + 3]-reconstruction	3	3



2

Fig. 1: Simplified structures of the reconstruction approaches.

Block structures of the conventional approach and the resulting cascaded system are shown in Fig. 1.

In the beamforming step, in theory different techniques could be applied. Here, the standard maximum-steering beamforming, as for example explained in [13], is used, as the principal goal is an increase of the SNR. The beamforming weights $w_{\mathrm{bf},m}$ are a function of the azimuth Doppler frequency f_{az} and the phase center distance $\Delta x_{\mathrm{bf},m}$ of the given (reconstructed) channel to the array center, computed as

$$w_{\mathrm{bf},m}\left(f_{\mathrm{az}}\right) = \frac{1}{M} \cdot \exp\left\{j\pi \cdot \frac{\Delta x_{\mathrm{bf},m}}{v_{\mathrm{s}}} \cdot f_{\mathrm{az}}\right\}.$$
 (4)

The phase center distance $\Delta x_{\mathrm{bf},m}$ of the *m*th reconstructed channel is hereby given as the mean phase center distance of all N channels used for its reconstruction, given by

$$\Delta x_{\mathrm{bf},m} = \frac{1}{N} \sum_{n=1}^{N} \Delta x_{n,m},\tag{5}$$

where $\Delta x_{n,m}$ is the distance of the *n*th sub-aperture's phase center to the array center for the *m*th channel subset.

III. PERFORMANCE ANALYSIS

The accuracy of the retrieved along-track deformation is mainly limited by two signal parameters: The SNR and the AASR of the acquisition. A detailed analysis of the impact of both effects on the along-track deformation retrieval can be found in [8].

A. SNR Analysis

The SNR is influenced by four main contributions: The system's noise power, the antenna pattern, the azimuth reconstruction filtering and the beamforming filtering. With noise power and antenna pattern assumed the same for all cases, the contributions that cause differences in the system's SNR characteristics are the reconstruction and the beamforming. The noise power level is computed by adding the scaled contributions of each of the independent realizations of the different channels in azimuth Doppler frequency domain.

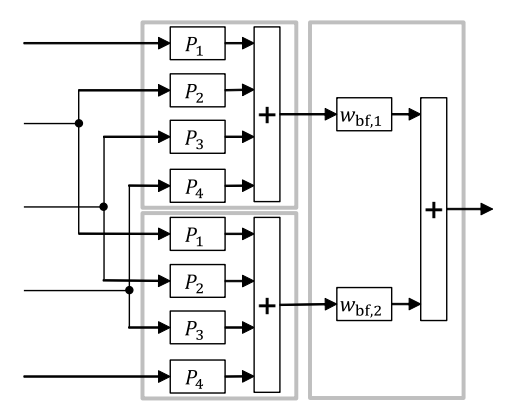


Fig. 2: Individual filtering steps for the [4 + 2]-reconstruction. The gray boxes represent the reconstruction and beamforming blocks as shown in Fig. 1b.

Fig. 2 shows the exemplary filter structure for the [4+2]-reconstruction. The system noise is assumed to be circular white Gaussian noise (CWGN) for each channel, scaled by the different filters and added incoherently. The total noise power p_{CWGN} follows as sum of the noise contributions $p_{\text{CWGN},n}$ of each channel n. To consider the scaling by the filters we compose a scaling vector $\mathbf{A}_M \in \mathbb{C}^{N_{\text{ch}} \times 1}$ to compute the noise power as follows

$$p_{\text{CWGN}} = \sum_{n=1}^{N_{\text{ch}}} p_{\text{CWGN},n}$$

$$= |\mathbf{A}_{M}|^{2} \cdot p_{\text{CWGN,ch}}$$

$$= |\mathbf{P}_{\text{casc}} \mathbf{w}_{\text{bf}}|^{2} \cdot p_{\text{CWGN,ch}}$$
(6)

where $p_{\mathrm{CWGN,ch}}$ is the input noise power level, assumed constant over the different channels. The scaling vector is created to represent the connections within the cascaded network and is computed from two scaling matrices $\mathbf{P}_{\mathrm{casc}} \in \mathbb{C}^{N_{\mathrm{ch}} \times M}$, and $\mathbf{w}_{\mathrm{bf}} \in \mathbb{C}^{M \times 1}$. Note that the following expressions omit the dependency on azimuth frequency f_{az} to improve readability. The structure of $\mathbf{P}_{\mathrm{casc}}$ represents the connections in the cascaded beamforming network. All elements on the jth full diagonal are equal to P_j , all other elements are 0. The vector \mathbf{w}_{bf} contains the beamforming weights. The scaling vector follows as the product of both, giving

$$\mathbf{A}_{M} = \mathbf{P}_{\text{casc}} \mathbf{w}_{\text{bf}} = \begin{bmatrix} P_{1} & 0 & \cdots & 0 \\ \vdots & P_{1} & \ddots & \vdots \\ P_{N} & \vdots & P_{1} & 0 \\ 0 & P_{N} & \vdots & P_{1} \\ \vdots & \ddots & P_{N} & \vdots \\ 0 & \cdots & 0 & P_{N} \end{bmatrix} \cdot \begin{bmatrix} w_{\text{bf},1} \\ \vdots \\ w_{\text{bf},M} \end{bmatrix}.$$

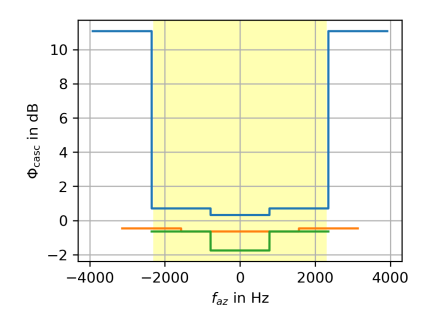


Fig. 3: Relative noise scaling over azimuth frequency for the test cases in Table II. Blue: Full reconstruction, orange: [4 + 2], green: [3 + 3]. The yellow area marks the bandwidth of a two-look burst.

As an example, the scaling vector \mathbf{A}_2 for the cascaded network in Fig. 2 is given as

$$\mathbf{A}_{2} = \begin{bmatrix} P_{1} & 0 \\ P_{2} & P_{1} \\ P_{3} & P_{2} \\ P_{4} & P_{3} \\ 0 & P_{4} \end{bmatrix} \cdot \begin{bmatrix} w_{\mathrm{bf},1} \\ w_{\mathrm{bf},2} \end{bmatrix} = \begin{bmatrix} P_{1}w_{\mathrm{bf},1} \\ P_{2}w_{\mathrm{bf},1} + P_{1}w_{\mathrm{bf},2} \\ P_{3}w_{\mathrm{bf},1} + P_{2}w_{\mathrm{bf},2} \\ P_{4}w_{\mathrm{bf},1} + P_{3}w_{\mathrm{bf},2} \\ P_{4}w_{\mathrm{bf},2} \end{bmatrix} . \quad (8)$$

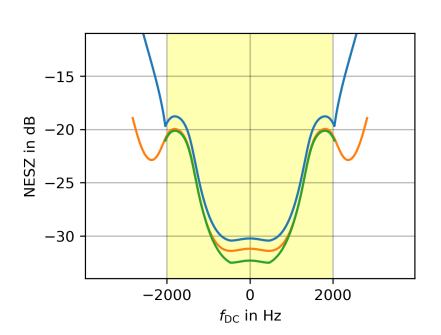
In the following we assume that the reconstruction filters P_n are scaled as given in [10], hence normalizing the signal power of the reconstructed signal with respect to the sum of all channels. The beamforming filters are assumed to scale the output to the power of a single input signal. Following the same rationale as in [10], we can then compute a relative noise scaling factor $\Phi_{\rm casc}$, given as

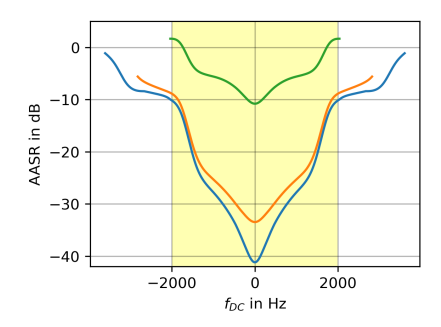
$$\Phi_{\rm casc} = \left(\frac{\rm SNR_{\rm casc}/SNR_{\rm ch}}{(\rm SNR_{\rm full}/SNR_{\rm ch})|_{\rm PRF_{\rm uni}}}\right)^{-1} = \frac{1}{N} \left|\mathbf{A}_{M}\right|^{2}. (9)$$

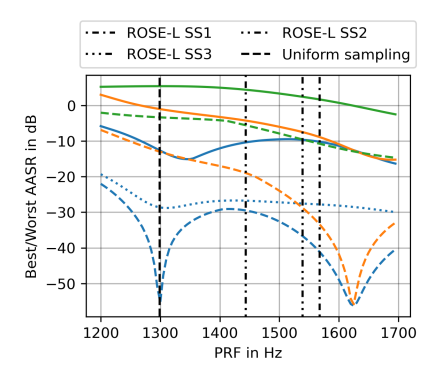
This factor gives the ratio of the noise scaling with respect to the signal scaling in the cascaded beamforming network compared to the full reconstruction case with uniform sampling with $\mathrm{PRF_{uni}}$, where $\mathrm{SNR_{casc}}$ and $\mathrm{SNR_{full}}$ are the SNR after cascaded reconstruction and full reconstruction with all channels, respectively, and $\mathrm{SNR_{ch}}$ is the SNR at the input of each channel.

Applying this analysis to the given ROSE-L case gives the results shown in Fig. 3. It can be clearly seen that both cascaded structures reduce the noise scaling, i.e., the SNR is improved in comparison to the full reconstruction. With the [4 + 2]-reconstruction, the noise is decreased by roughly 1.2 dB on the edges of the two-look bandwidth, furthermore it shows the most uniform performance, as with the given system parameters from Table I it operates close to uniform sampling. By using three reconstructed channels for beamforming, as in the [3 + 3]-reconstruction, the noise scaling can be reduced even more. Note, that due to the nature of the reconstruction filters, the relative noise scaling is constant within each spectral reconstruction interval of width $PRF_{\rm ch}$. The intervals are furthermore configured to be centered around $f_{\rm az}=0\,{\rm Hz}$.

Following the rationale of [8] and the parameters of Table I, the resulting noise-equivalent sigma zero (NESZ) of the focused ScanSAR signal as a function of the Doppler centroid







(a) NESZ over Doppler centroid frequency for the PRF given in Table I. The yellow shade marks the two-look burst span.

(b) AASR over Doppler centroid frequency for the PRF given in Table I. The yellow shade marks the two-look burst span.

(c) AASR over PRF. Solid: worst AASR within the two-look burst span, dashed: best AASR within the two-look burst span, dotted: worst AASR within the single-look burst span for reference.

Fig. 4: Signal performances within the focused image. Blue: full reconstruction, orange: [4 + 2], green: [3 + 3].

frequency $f_{\rm DC}$ can be computed by taking into account the antenna pattern and the noise power. The integration time over the aperture is also taken into account by averaging over the target bandwidth $B_{\rm target}$. The final NESZ curves are shown in Fig. 4a. Note that the SNR depends on the backscatter of the scene σ_0 and relates to the NESZ with the simple relation

$$SNR(f_{DC}) = \frac{\sigma_0}{NESZ(f_{DC})}.$$
 (10)

B. Azimuth Ambiguity Analysis

The AASR is another critical performance parameter for this analysis, as a decrease in the number of channels used for reconstruction implies the compensation of fewer azimuth ambiguities from the reconstructed signal. Hence, an increased AASR is to be expected from the cascaded networks in comparison to the full reconstruction. Similar to the analysis in [8], the AASR is evaluated for the cascaded networks. The results of this analysis, including ambiguities from within a total azimuth Doppler bandwidth of 15 · PRF_{ch}, are shown in Fig. 4b. As expected, the results show an increased AASR for reconstructions using less channels. Especially the cascaded network in [3 + 3]-configuration shows significantly higher ambiguity contributions than the full reconstruction. Being more sensitive to changes in the PRF than the SNR, the transferability of the results to different PRF values is evaluated in Fig. 4c. 1 Especially the cascaded networks will show larger ambiguity values for lower PRFs, while the full reconstruction shows less variations within the range of PRFs foreseen for ROSE-L.

C. Deformation Retrieval Accuracy Analysis

To retrieve the along-track deformation from the overlapping bursts, the same processing chain as in [8] is used. The retrieval chain generates complex interferograms of two

¹Due to the different number of ambiguities considered for the computation of the AASR, results in this article and in [8] differ slightly.

consecutive passes and exploits the differential interferometric phase (or spectral diversity phase) of the overlapping bursts to determine the along-track deformation. The performance of the retrieval is hereby limited by the signal quality, especially SNR and AASR. Note, that the SNR not only depends on the system, but also on the scene. For this analysis a range of different backscatter values is analyzed. The scene and processing parameters for the accuracy analysis are given in Table III.

TABLE III: Scene and processing parameters.

Reflectivity	σ_0	$-25\mathrm{dB}$ to $5\mathrm{dB}$
Temporal decorrelation	γ_{TEMP}	0.7
Number of looks	$N_{ m looks}$	50

The expected retrieval accuracy is now computed by combining the effects of SNR and AASR. Note, that the azimuth ambiguities are assumed to be uncorrelated between primary and secondary acquisitions, hence behaving as noise. Consequently, the coherence losses due to noise ($\gamma_{\rm SNR}$) and due to ambiguities ($\gamma_{\rm AASR}$) are given by

$$\gamma_{\text{SNR}}(f_{\text{DC}}) = (1 + \text{SNR}(f_{\text{DC}})^{-1})^{-1}$$
 (11)

$$\gamma_{\text{AASR}}(f_{\text{DC}}) = (1 + \text{AASR}(f_{\text{DC}}))^{-1}. \tag{12}$$

In the following, the coherence of the ScanSAR signal $\gamma(f_{\rm DC})$ is computed as a product of $\gamma_{\rm SNR}(f_{\rm DC})$ and $\gamma_{\rm AASR}(f_{\rm DC})$, as well as the temporal coherence $\gamma_{\rm TEMP}$, resulting in

$$\gamma(f_{\rm DC}) = \gamma_{\rm TEMP} \cdot \gamma_{\rm SNR}(f_{\rm DC}) \cdot \gamma_{\rm AASR}(f_{\rm DC}). \tag{13}$$

The accuracy of the retrieved along-track deformation is limited by the standard deviation of the two-look ScanSAR measurement $\sigma_{\rm 2LSC}$. It is a function of the coherences of both looks $\gamma_{L\{1,2\}}$, and is given by [8]

$$\sigma_{\rm 2LSC} = \frac{1}{\sqrt{2N_{\rm looks}}} \sqrt{\left(\frac{1 - \gamma_{L1}^2}{\gamma_{L1}^2} + \frac{1 - \gamma_{L2}^2}{\gamma_{L2}^2}\right)} \frac{v_{\rm g}}{2\pi\Delta f}, \quad (14)$$

where $v_{\rm g}$ is the platform velocity on ground and $N_{\rm looks}$ is the effective number of looks used in the multilooking of the

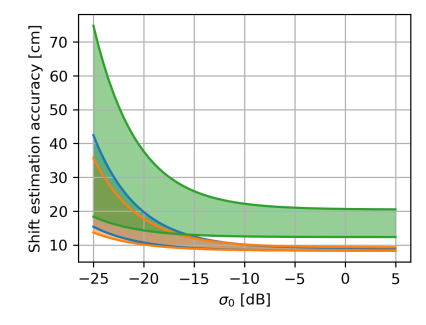


Fig. 5: Retrieval accuracies for parameters according to Table III. Each pair of lines represents the retrieval accuracies at burst center (upper line) and at the single-look burst edge halfway between center and two-look burst edge (lower line). Blue: full reconstruction, orange: [4 + 2], green: [3 + 3].

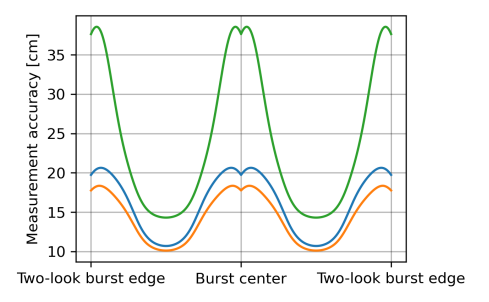


Fig. 6: Spatial variation of the retrieval accuracy for parameters according to Table III with $\sigma_0 = -20 \,\mathrm{dB}$. Blue: full reconstruction, orange: [4+2], green: [3+3].

interferograms. For ROSE-L, a multilooking with $N_{looks} = 50$ corresponds to a resolution of approximately $50 \,\mathrm{m} \times 50 \,\mathrm{m}$ in azimuth and ground range. The resulting retrieval accuracies for the different backscatter coefficients from Table III is shown in Fig. 5. As an example for the accuracy variation within the burst, the case of a low backscatter of $-20 \, dB$ is shown in Fig. 6. The results show, that for scenes with low backscatter, a small improvement in measurement accuracy can be achieved when using the [4 + 2]-reconstruction, for scenes with high backscatter, the full reconstruction performs slightly better than the cascaded approach. Under no circumstances, the [3 + 3]-reconstruction reaches the retrieval accuracies of the other two reconstruction approaches. We can identify a trade-off between mitigating the effects of azimuth ambiguities and the effects of system noise with the presented reconstruction approaches. If - and only if - the effect of the system noise on the retrieval accuracy is strong enough with respect to the effect of the azimuth ambiguities, a cascaded reconstruction approach can improve the alongtrack deformation retrieval. This trade-off also applies in case a modified antenna pattern is used, as suggested in [9]. In this case, the obtained accuracy values at the burst center and two-look burst edges will be more favorable due to the wider antenna pattern, at the price of a slightly increased standard deviation at the single look burst edges due to the overall increased NESZ.

Note that in case coherent ambiguities are assumed, in

contrast to what is implied in (13), no decorrelation due to ambiguities will occur. Instead, large phase biases can appear in the measured deformations [8].

IV. CONCLUSION

The results show that in theory a small improvement in measurement accuracy can be achieved by adapting the beamforming of the azimuth reconstruction. This effect is mostly relevant for scenes with small backscatter values, since in these cases the coherence of the acquisitions is dominated by the SNR. In other cases, the full reconstruction shows the better performance, due to its improved suppression of the azimuth ambiguities. In addition, in practice ambiguities will not be completely uncorrelated, as assumed in this performance analysis. This will lead to increased phase biases within the differential interferogram, complicating the unwrapping and affecting the interpretation of the results obtained with cascaded beamforming. The benefit of the cascaded beamforming could be more significant for systems with higher noise scaling or higher system NESZ than ROSE-L.

ACKNOWLEDGMENT

The authors would like to thank the two anonymous reviewers for their helpful comments and suggestions, which greatly improved the quality of the article.

REFERENCES

- T. J. Wright, B. E. Parsons, and Z. Lu, "Toward mapping surface deformation in three dimensions using InSAR," *Geophys. Res. Lett.*, vol. 31, no. 1, Jan. 2004.
- [2] A. Currie and M. A. Brown, "Wide-swath SAR," *IEE Proceedings F Radar and Signal Processing*, vol. 139, no. 2, pp. 122–135, 1992.
- [3] N. Yague-Martinez, P. Prats-Iraola, S. Wollstadt, and A. Moreira, "The 2-look TOPS mode: design and demonstration with TerraSAR-X," *IEEE Trans. Geosci. Remote Sens.*, vol. 57, no. 10, pp. 7682–7703, Oct. 2019.
- [4] R. Grandin, E. Klein, M. Métois, and C. Vigny, "Three-dimensional displacement field of the 2015 M8.3 Illapel earthquake (Chile) from across- and along-track Sentinel-1 TOPS interferometry," *Geophysical Research Letters*, vol. 43, no. 6, pp. 2552–2561, Mar. 2016.
- [5] N. Yague-Martinez and P. Prats-Iraola, "Accurate azimuth ground deformation estimation from Sentinel-1 time series," *IEEE Geosci. Remote Sens. Lett.*, vol. 19, pp. 1–5, Jan. 2022.
- [6] C. Liang and E. J. Fielding, "Measuring azimuth deformation with L-band ALOS-2 ScanSAR interferometry," *IEEE Trans. Geosci. Remote Sens.*, vol. 55, no. 5, pp. 2725–2738, May 2017.
- [7] M. Davidson, J. Kubanek, L. Iannini, R. Furnell, G. Di Cosimo, N. Gebert, D. Petrolati, D. Geudtner, and S. Osborne, "ROSE-L - the Copernicus L-band synthetic aperture radar imaging mission," in *Proc. IEEE Int. Geosci. Remote Sens. Symp. (IGARSS)*, 2023, pp. 4568–4571.
- [8] S. Trumpf, P. Prats-Iraola, and A. Moreira, "Along-track deformation retrieval performance with the ROSE-L multichannel SAR system using two-look ScanSAR," *IEEE Trans. Geosci. Remote Sens.*, vol. 63, pp. 1– 15, Apr. 2025.
- [9] S. Perna, F. Longo, S. Zoffoli, M. Davidson, L. Iannini, and R. Lanari, "A conceptual performance study on a two-look ScanSAR mode configuration for the forthcoming ROSE-L mission," *IEEE Trans. Geosci. Remote Sens.*, vol. 62, pp. 1–18, 2024.
- [10] N. Gebert, G. Krieger, and A. Moreira, "Digital beamforming on receive: Techniques and optimization strategies for high-resolution wide-swath SAR imaging," *IEEE Trans. Aerosp. Electron. Syst.*, vol. 45, no. 2, pp. 564–592, Apr. 2009.
- [11] S. J. Trumpf, P. Prats, and A. Moreira, "Investigations on a two-look ScanSAR mode for along-track deformation measurements with ROSE-L," in *Living Planet Symposium*, Jun. 2025.
- [12] J. C. Curlander and R. N. MacDonough, Synthetic aperture radar, ser. A Wiley Interscience publication. New York, NY [u.a.]: Wiley, 1991.
- [13] J. R. Guerci, Space-time adaptive processing for radar, ser. Artech House radar library. Boston: Artech House, 2003.